A Recursive Filter for Phase Velocity Assisted Shape-based Tracking of Cardiac Non-rigid Motion*

John C. McEachen II[†], François G. Meyer[◇,‡], R. Todd Constable[‡], Arye Nehorai[†], and James S. Duncan[†,‡]

Image Processing and Analysis Group
Departments of [†]Electrical Engineering, [◇]Mathematics, and [‡]Diagnostic Radiology
Yale University, P.O. Box 208042, New Haven, CT 06520-8042

Abstract

A framework for tracking pointwise periodic non-rigid motion of the heart's left ventricular (LV) wall is presented which incoporates information from two different magnetic resonance imaging (MRI) techniques. New developments in phase-contrast cine MR imaging have produced spatial maps of instantaneous velocity that have proven accuracy within the myocardium, or wall, of the heart. This information is combined with shape-based matching techniques to provide improved estimates of trajectories, especially in regions where shape information is limited. These raw trajectories act as input to a recursive least squares (RLS) filter which applies the constraints of temporal periodicity and spatial smoothness for the final estimate. The results of the RLS filter are compared with the motion of actual implanted markers. Comparisons are also made between exclusively shape-based filtered and phase-contrast enhanced trajectory estimates using both phantom and actual canine heart MR images.

1 Introduction

Tracking non-rigid motion, particularly in medical image sequences, has received considerable interest within the computer vision community in recent years [1]. Cardiac image analysis has seen a large share of this effort specifically in identifying myocardial damage due to heart disease. The requirement for non-invasive diagnosis of regional cardiac function has confounded the problem, however, leaving potential researchers with no concrete landmarks to assist them in their analysis. Cardiac MRI analysis in particular does afford the researcher some useful constraints which we explore in this paper. Specifically, the periodic nature of the cardiac cycle is well suited for the tools of harmonic analysis. We present a temporal model based on a sum of sinusoids that forms the basis for our (RLS) tracking filter. Additionally, new developments in phase-contrast cine MRI encoding have led to accurate spatial maps of velocity within the myocardium, or wall, of the LV. We employ a finite-element based mesh across the myocardium to capture the global or regional motion of the LV, then use this information to assist our traditional shape-based correspondence method ([2]) in refining our point-wise estimate of the frame-to-frame trajectories. We show that this method is particularly useful in regions with limited shape variation. The work in this paper is based on previous efforts in [3] and [4].

1.1 Background

The ability to track points on object surfaces over time has been a principal goal of both rigid and non-rigid motion research in the field of computer vision. Snakes, or active contour models, have been the primary focus of many recent efforts (*e.g.* - [5]). All of these methods are frame-to-frame iterations and do not take advantage of any temporal trends. One method using a deformable model, [6], uses vibrational modes to parameterize its object of concern. However, these harmonics are not to be confused with the type of harmonics used in our method. The vibrational modes do not take into account any periodic nature associated with either the contour or its periodic deformation.

The technique of harmonic analysis and enhancement is well established [7]. The major thrust of research in this area has focused on estimating parameters of one-dimensional signals where the fundamental frequency is unknown (*e.g.* - [8]). Little has been explored in the area of enforcing periodic constraints which adds to the significance of the method presented below.

The problem of quantifying regional LV wall function is not new to the field of cardiology either. MR signal tagging ([9]) has seen much recent interest, however the spatial resolution of the measured motion depends on the pixel size of the tags making point-wise tracking difficult. Also, these methods have difficulty imaging the entire cardiac cycle.

Phase contrast approaches to MRI motion analysis have shown promising gains over previous MR signal encoding techniques such as spin tagging. Van Dijk ([10]) first suggested use of the NMR phase to record cardiac wall ve-

*This research is supported in part by NIH Grant T15 LM07056 from the National Library of Medicine and by NIH Grant R01HL44803 from the National Heart, Lung and Blood Institute. The work of A. Nehorai was supported by the Air Force Office of Scientific Research under Grant F49620-93-1-0096, the Office of Naval Research under Grant N00014-91-J-1298 and the National Science Foundation under Grant MIP-9122753.

0-8186-7042-8/95 $4.00

locity measurements using a spin echo gated MR imaging sequence. Since then methods have been developed for tracking cardiac wall motion based solely on these velocity maps ([4]). In cardiac MRI analysis, these velocity maps have been shown to be highly accurate for regions embedded in the myocardium. Unfortunately, pixels near the boundaries of the LV become influenced by the spectral content of surrounding non-homogeneous material resulting in a considerable number of outliers. Thus the phase-contrast method in itself is not suitable for tracking point-wise trajectories along the LV wall. It does, however, provide us with considerable general information regarding global LV motion. It is in this manner that we incorporate the information into our method below.

1.2 Assumptions

Our approach to tracking and quantifying the motion of the LV wall is based upon several important assumptions. First, we assume that the endocardial contours must be extracted to provide an estimate of the location of the LV wall in each image frame over an entire cycle. Second, we assume that a set of reliable shape tokens can be derived from each of the extracted boundaries. Finally, we assume that motion is such that the tokens change only a small amount from frame to frame. Given these assumptions we have developed an algorithm for computing non-rigid object motion from a sequence of images.

2 Predicting Displacements using Dense Velocity Maps

The availability of dense 2-D velocity maps provides new options for estimating the correspondence between material points over time. We draw on the insight of continuum mechanics and finite element analysis to extract parameters of motion for vertices lying on the boundary. The motion estimate for these points is then refined using our traditional shape-based matching method. The idea of exploiting velocity and shape information has also been proposed in [11]. We emphasize the case where velocity measurements are obtained by phase-contrast MRI, although we note that velocities can be directly estimated from the spatiotemporal changes of the intensity function [12].

2.1 Deformation and Velocity Model

Let $\mathbf{u}(\mathbf{x},t) = (u(x,y,t), v(x,y,t))$ be the Eulerian velocity at the position $\mathbf{x}$ and at time t. Let $\mathbf{L}$ be the velocity gradient tensor [13]. In our analysis of the deformable motion we assume that the velocity gradient is locally homogeneous. However we note that $\mathbf{L}$ will change from one neighborhood of the myocardium to another. This physical assumption of local homogeneity results in a locally affine model. For any point $\mathbf{x}+\delta\mathbf{x}$ in a small neighborhood around $\mathbf{x}$ we have

$$\mathbf{u}(\mathbf{x}+\delta\mathbf{x},t) = \mathbf{u}(\mathbf{x},t) + \mathbf{L}\delta\mathbf{x} \qquad (1)$$

Finally, the entire velocity field inside the myocardium is characterized as a continuous piecewise affine vector field. To construct a satisfactory description of the velocity field we subdivide the domain into triangles in 2-D. Let $\mathcal{P}$ be the space of continuous piecewise linear functions in two arguments associated with the partition. We have $\mathbf{u} \in \mathcal{P}\times\mathcal{P}$. Let N be the number of nodes of the partition. A local basis of $\mathcal{P}$ is composed of the collection $(\xi_k)_{k=1\ldots N}$, where ξ_k is the linear function which takes the value 1 at the vertex k and vanishes on all other nodes [14]. We can now express our model of the entire velocity field inside the myocardium. We have

$$(u,v)(t) = \left(\sum_{k=1}^{N} u_k\xi_k, \sum_{k=1}^{N} v_k\xi_k\right)(t) \qquad (2)$$

The expansion of the velocity field in this local basis sets up a one-to-one correspondence between the dense motion of the material points inside the medium, and the motion of the nodes of the mesh.

2.2 Regularization of the velocity

Phase contrast MRI velocities are often noisy. Significant outliers may appear on regions near the boundary of the myocardium, as shown in figure 1a, which are caused in part by the presence of the turbulent motion of the blood in the cavity. We have developed a method for the approximation of an observed vector field by a vector field of continuous piecewise linear functions in two variables. Given an observation of the velocity field $\mathbf{u} = (u,v)$, our goal is to estimate the best approximation, $\mathbf{p} = (p,q)$ of $\mathbf{u}$ in $\mathcal{P}\times\mathcal{P}$ that minimizes the error

$$\int_\Delta (\mathbf{p}-\mathbf{u})^2 = \int_\Delta (p-u)^2 + \int_\Delta (q-v)^2 \qquad (3)$$

Let (α,β) be the coordinates of the expansion of (p,q) in the local basis $(\xi_k)_{k=1\ldots N}$. The problem (3) can be expressed as

$$\min_{\alpha_i,\beta_j} \int_\Delta \left(\sum_{i=1}^{N}\alpha_i\xi_i - u\right)^2 + \left(\sum_{j=1}^{N}\beta_j\xi_j - v\right)^2 \qquad (4)$$

(4) is a classic least-squares problem. Taking the partial derivative with respect to α_i, the solution α of (4) is given by the normal equations. Figure 1a shows the phase contrast velocity field in a small region around the myocardium. We note the turbulent flow in the blood pool, and the noisy vectors outside in the pericardial space. Such erroneous velocities should seriously hamper any tracking algorithm based on these data. Figure 1b shows the result of the approximation algorithm. While keeping the same pattern and structure, the flow field is smoother. Noisy vectors have been discarded.

2.3 Integration of the velocity

Given the smooth estimate of the Eulerian velocity field $\mathbf{p} \in \mathcal{P}\times\mathcal{P}$ at time t_i, we predict the position of the boundaries of the myocardium at time t_{i+1}. Let C_i be the position of any of the two boundaries of the myocardium (the endocardium or the epicardium) at time t_i. The trajectory of the boundary is given by the mapping $\mathbf{x}$ which is the solution of the differential equation

$$\frac{\partial\mathbf{x}}{\partial t}(\mathbf{X},t) = \mathbf{p}(\mathbf{x}(\mathbf{X},t),t), \qquad \forall\,\mathbf{X}\in C_i$$

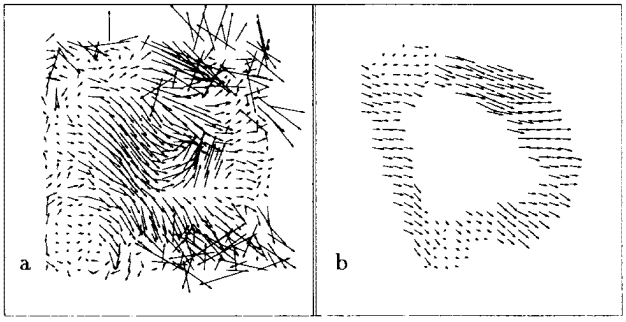

Figure 1: (a) Phase contrast MRI velocity field around the myocardium. (b) Continuous piecewise affine approximation of the velocity field shown in (a).

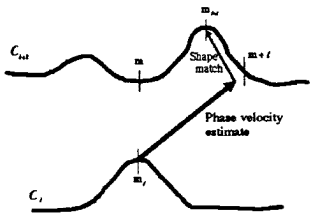

Figure 2: Combining the displaced estimate of the phase velocity map with shape-based matching. The thick arrow indicates the displacement estimated by processing phase velocity. The thin arrow indicates the resulting shape match extended from the phase velocity estimate. $\mathbf{m} + t$ indicates where the search window, $W(s_i)$, is centered.

Given the position $\mathcal{C}_i$ of the boundary at time t_i we compute the position at the next instant using a first order Euler method. In general the result of the integration will not completely coincide with $\mathcal{C}_{i+1}$. Geometric cues such as curvature can refine this initial estimate of displacement between two successive frames as explained below.

3 Shape-based Refinement

In the next two sections, we refer to the the image sequence-derived contours that define the moving LV boundary with the intent of computing flow vector fields that will aid in the tracking of point trajectories of contour pairs. We note that we will consider two contours, $\mathcal{C}_i$ and $\mathcal{C}_{i+1}$, derived from successive image frames representing times t_i and t_{i+1} in an image sequence. These are part of a discrete set of contours representing point sets that exist over a set of T image frames in a two-dimensional Euclidean image space, i.e. $\mathcal{C}_i \subset \mathcal{R}^2$, $\forall i \in [0, ..., T]$. We will use m_i and m_{i+1} to index equal, unit-length samples along the discrete versions of $\mathcal{C}_i$ and $\mathcal{C}_{i+1}$.

3.1 Local Segment Matching

Correspondences between points on the initial contour $\mathcal{C}_i$ and points on a successive contour $\mathcal{C}_{i+1}$ in the sequence are found by matching shape properties of contour segments surrounding each of the points in a manner similar to [2]. In this method, a fixed-size portion of the contour at time t_{i+1} was used to define the search window, $W(s_i)$, for any point on the contour found at time t_i. This portion of $\mathcal{C}_{i+1}$ chosen for $W(s_i)$ was that centered on the point of nearest Euclidean distance to the initial point of $\mathcal{C}_i$. In our current method, the displacement estimate given by the phase contrast velocity flow map is used to guide the positioning of $W(s_i)$ on $\mathcal{C}_{i+1}$. This is done simply by taking the point on $\mathcal{C}_{i+1}$ of nearest Euclidean distance to *the Euclidean location* of the displaced estimate, $(x, y)(t_{i+1}|t_i)$, given by the integration of the phase velocity map for the initial point on $\mathcal{C}_i$. The search window, $W(s_i)$, is then centered on this point as shown in figure 2. We hypothesize that this approach allows us to incorporate global torque and translation given by phase velocity information with local shape continuity correspondence.

We set up the correspondence problem as one of finding the points on the contour at time t_{i+1} that best match each of the $N + 1$ points m_i. Assuming approximately equal length contours and coincident indices, this problem can be viewed as finding the deviation from a one-to-one mapping of the mapping of m_i into m_{i+1}, $\forall m_i \in [0, N]$. Thus, we will use the notation m_{i+1}^{shape} to denote the point on the contour at time t_{i+1} that best matches each monotonically ordered point m_i $(= m)$. Furthermore, we note that $m_{i+1}^{shape} = m + \delta_m^{shape}$, where δ_m^{shape} is the optimal deviation from the original one-to-one mapping at original sample point m. See also [2].

For the method described below, we find it useful to define a vector $\mathbf{m}_{i+1}^{shape}$ that is of dimension $N + 1$ and is a stacking of the correspondences found for each original $m_i = m = [0, N]$. In other words $\mathbf{m}_{i+1}^{shape} = \mathbf{m} + \left[\delta_0^{shape}\, \delta_1^{shape}, \ldots, \delta_m^{shape}, \ldots, \delta_N^{shape}\right]^T$.

3.2 Confidence Measures

The need for confidence measures is brought about by notions of: 1) how matches in any one region are treated in the sense of their relative strength when compared with matches created in other local regions, and 2) how decisions are handled in regions where there are many plausible matches. Thus, the strength and uniqueness of a match is used to help drive the solution of the overall flow field. Guided by the work in [15], we define two confidence measures, both based upon the profile of the error measure within each search region $W(m_i)$, that address these issues of strength and uniqueness.

4 Flow Vector Computation

We seek to find a vector flow field that corresponds points on two contours found from two consecutive temporal frames in an image sequence by compromising between adhering to the points where the local shape of the contours best match and the model that adjacent points on the contour move smoothly. Based on this model, the smoothest possible mapping of m_i onto m_{i+1} for all m is a linear one-to-one mapping. We adhere to this by incorporating a term dependent on the second derivative of the mapping into a cost function. This function can be posed

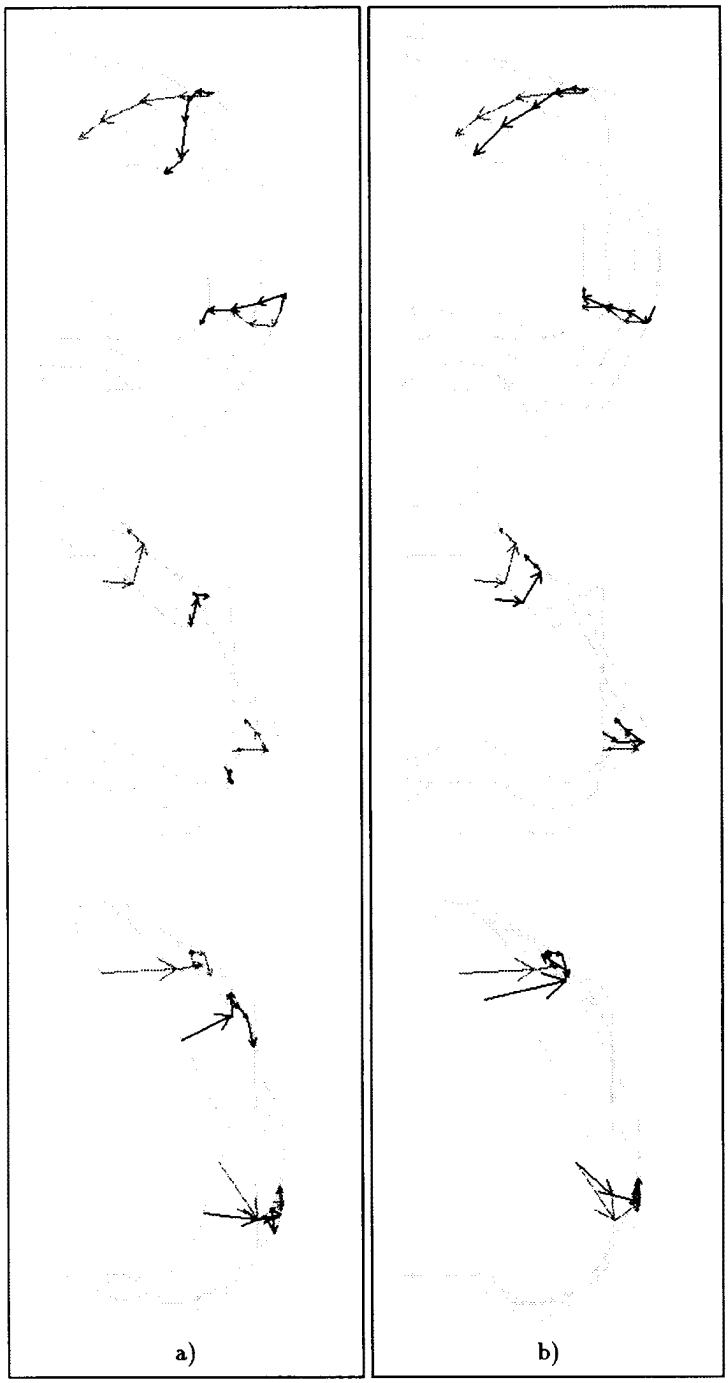

Figure 3: a) Corresponding trajectories estimated with a frame-to-frame shape-based tracking algorithm without any periodicity constraints (shown in black) compared with marker trajectories (shown in grey). (Top) Frames 1-6. (Middle) Frames 6-10. (Bottom) Frames 10-16. b) Corresponding trajectories estimated with the recursive filter presented in this paper (in black) compared with marker trajectories (in grey). (Top) Frames 1-6. (Middle) Frames 6-10. (Bottom) Frames 10-16.

conveniently in vector notation. We define a diagonal confidence matrix, $\mathbf{C}$, where diagonal elements are equal to the product of the two confidences for a given m_i. If we use $\mathbf{m}_i^{shape}$ to denote the discrete shape-based correspondences stacked as a vector, and in similar fashion use $\mathbf{m}_i$ to reflect variation in correspondences and $\mathbf{m}_i^*$ to denote the optimal correspondence set, we can express the cost function as follows:

$$\begin{aligned} F &= (\mathbf{m}_i - \mathbf{m}_i^{shape})^T \mathbf{C}_{i+1} (\mathbf{m}_i - \mathbf{m}_i^{shape}) \\ &\quad + (\mathbf{D}\mathbf{D}\mathbf{m}_i)^T (\mathbf{D}\mathbf{D}\mathbf{m}_i) \end{aligned} \tag{5}$$

where $\mathbf{D}$ is a first order differential operator and $\mathbf{m}_i^{shape}$ is the initial shape-based mapping vector.

It can be shown that the matrix $(\mathbf{C}+\mathbf{D}^T\mathbf{D}^T\mathbf{D}\mathbf{D})$ is positive definite. By multiplying, combining, and eliminating non-related terms (see [3]) we find the optimal estimate for $\mathbf{m}_{i+1}$ that minimizes F is given as:

$$\mathbf{m}_{i+1}^* = (\mathbf{C}_{i+1} + \mathbf{D}^T\mathbf{D}^T\mathbf{D}\mathbf{D})^{-1}\mathbf{C}_{i+1}\mathbf{m}_{i+1}^{shape} \tag{6}$$

The vector $\mathbf{m}_{i+1}^*$ can be viewed as the nearest local minimum on this optimization surface which qualitatively represents a vector flow field that contains a compromise between 1) the best local matches for all points on the first contour to the second contour, with each match being weighted according to uniqueness of the shape in the match region and, 2) requiring each of these vectors to have a magnitude and direction that smoothly agrees with its spatially neighboring vectors. Additionally, posing the optimization problem in the contour space implicitly constrains the displacement vectors to the contours themselves.

5 The Temporal Model

We note that our representation of endocardial motion is periodic in both contour space ($m_i \in [1, N]$) and time ($i \in [1, T]$). This is a unique aspect of the problem of tracking LV wall motion which has not been exploited. If we consolidate all our continuous mapping functions into one two-dimensional function, we can express any discrete point on the entire manifold as follows:

$$m_i = \sum_{p=1}^{P}\sum_{r=1}^{R} C_{p,r}\sin(p\omega_o m + r\tau_o t + \psi_{p,r}) \tag{7}$$

where $\omega_o = \frac{2\pi}{N}$ is the fundamental frequency over the space of the contour and $\tau_o = \frac{2\pi}{T}$ is the fundamental frequency of the cardiac cycle over time. The index p represents harmonics of ω_o, and similarly r indexes τ_o. P and R represent the highest significant harmonics of ω_o and τ_o respectively. $C_{p,r}$ and $\psi_{p,r}$ are the amplitude and phase of the (m,n)th harmonic component of $\phi(s,t)$ respectively.

For the purpose of developing a system equation, (7) can be converted into a vector product using $\mathbf{m}_i = \Xi_i\eta$ for a given frame i; where $\mathbf{m}_i$ is the mapping function to frame i, Ξ_i is of size $N \times 2PR$ and represents the cosine and sine terms for a given i, and η is of size $2PR \times 1$ and represents phases and amplitudes of harmonic components.

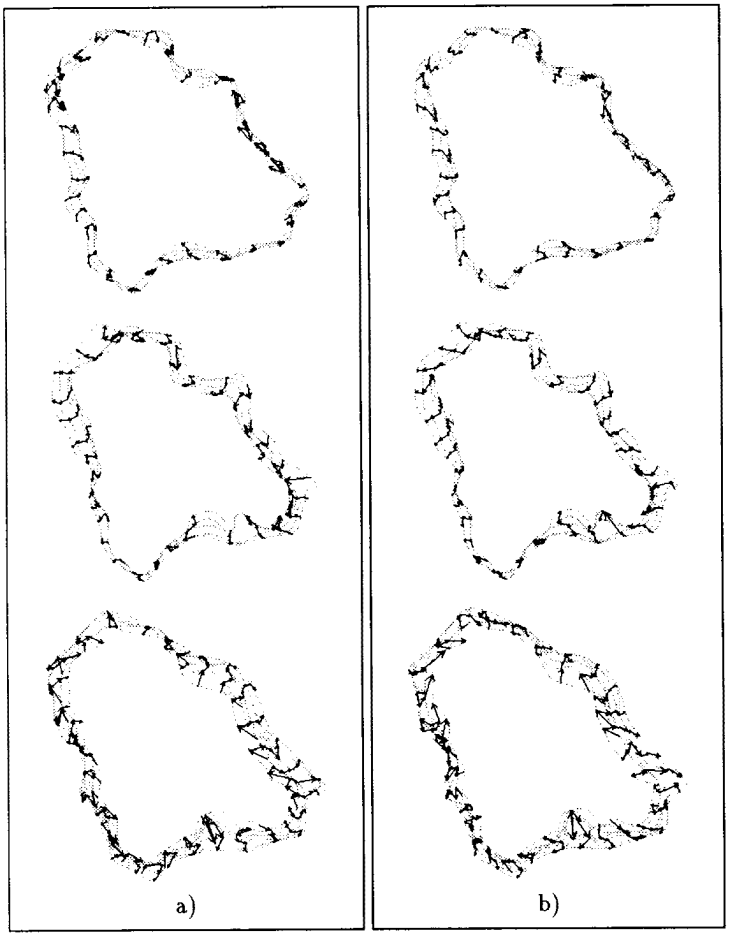

Figure 4: a) Tracking the endocardial wall (short axial view) in another canine LV study using our shape-based RLS filter with no phase contrast velocity information. (Top) Frames 1-6. (Middle) Frames 6-11. (Bottom) Frames 11-16. **b)** Tracking the same study as in a), but this time incorporating the phase velocity information shown in figure 1a into the filtering process. (Top) Frames 1-6. (Middle) Frames 6-11. (Bottom) Frames 11-16.

6 Recursive Filtering

Having defined a relationship between the "observed" shape-based matches and our desired mapping solution as well as an extended temporal model for this system, we now derive an observation equation and subsequent iterative filter to exploit these properties. If we assign $\mathbf{H} = (\mathbf{C} + \mathbf{D}^T\mathbf{D}^T\mathbf{D}\mathbf{D})^{-1}\mathbf{C}$, and note that $\mathbf{H}$ is positive definite, we can combine (6) with $\mathbf{m}_i = \Xi_i\eta$ as follows:

$$\mathbf{m}_i^{shape} = \mathbf{H}_i^{-1}\Xi_i\eta + \nu_i \tag{8}$$

ν_i represents observation noise at frame i.

We use a recursive least squares (RLS) filter to determine the final estimate:

$$\hat{\eta}_i = \hat{\eta}_{i-1} + \mathbf{K}_i(\mathbf{m}_i - \mathbf{G}_i\hat{\eta}_i) \tag{9}$$

where $\mathbf{G}_i = \mathbf{H}_i^{-1}\Xi_i$ and $\mathbf{K}$ is the system gain matrix.

The solution mapping is retrieved after T iterations of the RLS filter have been computed by carrying out $\hat{\mathbf{m}}_i^* = \Xi_i\hat{\eta}\ \forall i$. This final mapping represents a shape-driven, spatially and temporally smooth, and periodically constrained solution to the posed problem.

7 Results

To illustrate our algorithm, we employ it in analyzing a set of sixteen contours from MR images of the complete cycle (end-diastole (ED) to end-systole (ES) and back to ED) of a healthy canine LV. In figure 3, we highlight the track of two markers that were implanted on the LV wall of this same canine heart. Phase contrast velocity information was not available in this experiment so we will concentrate on verifying the usefullness of our filtering approach. Figure 3a compares the corresponding pair of trajectories (i.e. - those with the same starting point) obtained using our old shape-based tracking algorithm without any temporal filtering. Finally, figure 3b compares the results of our new recursive filtering algorithm for the same trajectories.

We observe that the old shape-based tracking algorithm diverges from the actual track, especially in the case of the upper trajectory which completes the cycle far from it's initial starting position. On the other hand, when our periodicity constraint is incorporated the estimated trajectory is much closer to the actual track and in many instances exactly matches it. Even in situations where the tracks have diverged we note that filtered estimate still follows the general flow of the actual track.

Figure 4 illustrates the gain in performance achieved by using phase velocity information. The shape-based method alone (figure 4a) does a very plausible job of tracking the actual endocardial contours. We then examine the results from our combined shape-based, phase velocity approach in figure 4b for comparison and note the improvement in areas where little shape variation occurs. Finally, in figure 5, we compare composite graphics from tracking the phase velocity information alone using smoothed contours to those trajectories obtained from our combined method. We note that even when we use a smooth restricted set of contours, the phase velocity flow alone does not do any better. In fact in areas of high motion, the accumulated error becomes significant, leaving the ending trajectory far from its starting point. This is partly because the velocity map in this instance is much noisier as shown in figure 1a above. When we combine the two methods though, we see a marked improvement over both estimates. Examining the contours illustrates that in instances where strong features exist, the shape match refinement helps maintain adherence to the feature, but in areas where little shape information exists the phase velocity maps force the trajectories in the correct direction.

8 Summary

We have a presented a novel tracking algorithm for analyzing the motion of periodically deforming contours such as those from images of the endocardial LV wall. This algorithm uses several techniques that have not seen prior use in computer vision literature, specifically velocity maps from phase-contrast cine MRI and multi-dimensional harmonic analysis of deforming contours. Using these com-

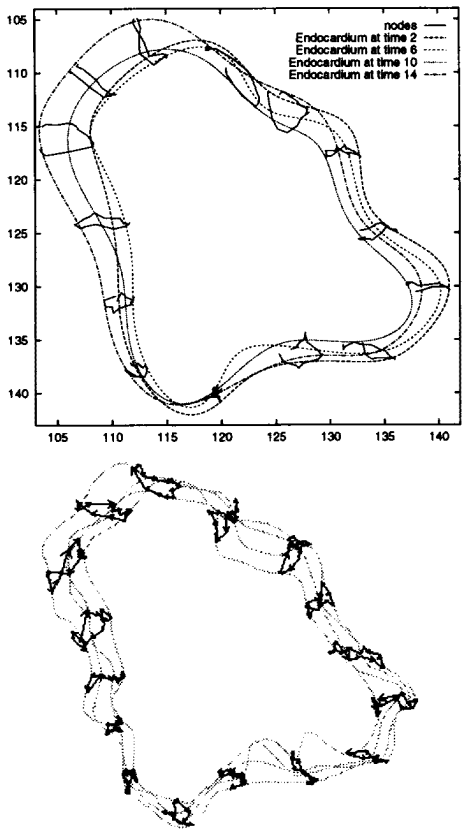

Figure 5: (Left) Results from tracking the same canine study as in figure 4 using strictly phase velocity information from the deforming mesh. Note for this example, very smooth versions of the contours are used to avoid integrating outliers into the solution. (Right) Composite graphic of results from figure 4 combining phase velocity and shape information using actual contours. In both graphics only contours from frames 2, 6, 10 and 14 of the 16 frame sequence are shown to avoid cluttering the graphic.

bined techniques we developed a method of filtering our phase velocity-driven, shape-based mapping function to obtain a more desirable, smoothly varying mapping function. This final mapping function is the result of a process that combines knowledge of physical flow, feature adherence, spatial smoothness and temporal trends into one iterative filter.

We presented results based on actual MR data that show considerable promise when compared to the trajectories of implanted markers and previous trajectory estimates. Of course, we cannot expect to achieve precisely the same motion correspondences since the true trajectory extends in three spatial dimensions, however we are encouraged by these results and intend to integrate them with concurrent work of our group in matching three-dimensional surfaces.

We showed how incorporation of information from phase velocity analysis can be used to guide the shape correspondence process, especially in areas where shape variation is limited. This method of integrating different modes of MR data shows considerable potential and will be pursued extensively in the future.

Acknowledgment

The authors would like to thank Dr. Albert Sinusas and Don Dione of the Department of Cardiology, Yale School of Medicine, for performing the experiments used to extract the phase-contrast cine MR data.

References

[1] Dmitry Goldgof and Raj Acharya, editors. *IEEE Workshop on Biomedical Image Analysis*, Seattle, WA, June 1994. IEEE Computer Society Press.

[2] J. S. Duncan, R. L. Owen, L. H. Staib, and P. Anandan. Measurement of non-rigid motion using contour shape descriptors. In *Computer Vision and Pattern Recognition*, pages 318–324, Lahanai, Maui, HI, June 1991. IEEE.

[3] John C. McEachen II, Arye Nehorai, and James S. Duncan. Analysis of cardiac motion with recursive comb filtering. In *Mathematical Methods in Medical Imaging III*, pages 46–57, San Diego, CA, July 1994. SPIE.

[4] R. Todd Constable, Kristina M. Rath, Albert J. Sinusas, and John C. Gore. Development and evaluation of tracking algorithms for cardiac wall motion analysis using phase velocity mr imaging. *Magnetic Resonance in Medicine*, 32:33–42, 1994.

[5] Demetri Terzopoulos and Richard Szeliski. Tracking with kalman snakes. In Andrew Blake and Alan Yuille, editors, *Active Vision*, pages 3–20, Cambridge, MA, 1992. The MIT Press.

[6] Alex Pentland, Bradley Horowitz, and Stan Sclaroff. Non-rigid motion and structure from contour. In *IEEE Workshop on Visual Motion*, pages 288–293, Princeton, NJ, October 1991. IEEE Computer Society.

[7] S. M. Kay and S. L. Marple Jr. Spectrum analysis - a modern perspective. *Proceedings IEEE*, 69:1380–1419, Nov. 1981.

[8] Arye Nehorai and Boaz Porat. Adaptive comb filtering for harmonic signal enhancement. *IEEE Trans. on ASSP*, 34(5):1124–1138, Oct. 1986.

[9] E. Zerhouni and et. al. Tagging of the human heart by multiplanar selective RF saturation for the analysis of myocardial contraction. In *Abstracts of the Ann. Meeting of the Soc. of MR in Imaging*, page 10, San Francisco, 1988.

[10] P. van Dijk. Direct cardiac nmr imaging of heart wall and blood flow velocity. *J. Comput. Assist. Tomogr.*, 8:429–436, 1984.

[11] F.G. Meyer, R. T. Constable, A. J. Sinusas, and J. S. Duncan. Tracking myocardial deformation using spatially-constrained velocities. In *XIVth International Conference on Information Processing in Medical Imaging, IPMI'95, June 26-30, 1995, Ile de Berder, France.* Kluwer Press, 1995.

[12] S.M. Song, R.M. Leahy, D.P. Boyd, B.H. Brundage, and S. Napel. Determining cardiac velocity fields and intraventicular pressure distribution from a sequence of ultrafast CT cardiac images. *IEEE Trans. on Medical Imaging*, Vol. 13, No.2:386–397, June 1994.

[13] A.J.M. Spencer. *Continuum Mechanics.* Longman, 1980.

[14] E.B. Becker, G.F. Carey, and J.T. Oden. *Finite Elements, An Introduction, Volume I.* Prentice-Hall, 1981.

[15] P. Anandan. A computational framework and an algorithm for the measurement of visual motion. *International Journal of Computer Vision*, 2:283–310, 1989.